Transport in Chaotic Magnetic Fields

by

Francisco Holguin

Submitted to the Department of Physics
in partial fulfillment of the requirements for the degree of

Bachelor of Science in Physics

at the

MASSACHUSETTS INSTITUTE OF TECHNOLOGY

June 2016

Signature redacted

Author .....
Department of Physics
May 13, 2016

Signature redacted

Certified by .....
Abhay K. Ram
Thesis Supervisor
MIT Plasma Science and Fusion Center

Signature redacted

Accepted by ....
Nergis Mavalvala
Senior Thesis Coordinator
Department of Physics

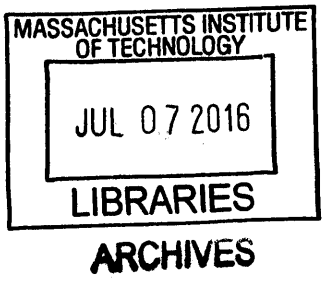

Transport in Chaotic Magnetic Fields

by

Francisco Holguin

Submitted to the Department of Physics
on May 13, 2016, in partial fulfillment of the
requirements for the degree of
Bachelor of Science in Physics

Abstract

Many astrophysical environments are thought to contain force-free magnetic fields. The sine field is an example of a force-free, helical magnetic field, whose field lines are chaotic over the entire space. In this thesis, we examine the transport properties of magnetic field lines and particles in three related systems: the sine field, the sine field superimposed with a constant background field, and a time varying sine field. We also compare results with the Arnold-Beltrami-Childress (ABC) field. In the time-independent sine field, we find that particles exhibit chaotic motion, shown by a non-zero distribution of Lyapunov exponents (LE). While for low energies the asymtotic LE do not depend on initial particle position or angle with respect to the local magnetic field line, these parameters are important for higher energies. On larger time scales, we find that an ensemble of particles undergoes close to normal diffusion for low energies and superdiffusion for high energies. This contrasts with the superdiffusion found at low energies with the ABC field. Additionally, we find that adding a constant magnetic introduces a saturation time scale in the cross field diffusion. The saturatino can be both temporary or more long term. We find that the low energy particle motion is ballistic. In contrast, for higher energies we find widely varying behavior, ranging from superdiffusion to normal diffusion. At the highest energies though, the behavior becomes uniformly superdiffusive. Futhermore, we introduce a simple sinusoidal time variation into the sine field. We find that in the pure sine field, the particle energy experiences subdiffusion throughout all the time scales. With the constant field added, there is only energization at long timescales, and although not completely conclusive, it looks to eventually undergo normal diffusion in energy.

Thesis Supervisor: Abhay K. Ram
Title: MIT Plasma Science and Fusion Center

Acknowledgments

I would like to thank Abhay K. Ram for his guidance and support in supervising this research.

Contents

Chapter 1

Introduction

Many different astrophysical plasma environments are thought to contain force-free magnetic fields. A force-free magnetic field arises when the plasma pressure is small compared to the magnetic pressure. In particular, the force free approximation holds for conditions in the solar upper chromosphere and corona [19]. Because of the ubiquity of these fields, it is important to study the spatial structure of these magnetic fields and their effect on the motion, or spatial transport, of charged particles in such plasmas. In addition, these astrophysical plasmas contain charged particles that have been accelerated to energies much greater than the thermal energy. As a consequence, it is also of interest to study the energization of these particles.

Force-free magnetic fields have the property

$$\nabla \times \mathbf{B} = \lambda \mathbf{B} \tag{1.1}$$

with λ in general being an arbitrary function of position. The force-free magnetic fields are mathematically equivalent to Beltrami flows [9], where $\nabla \times \mathbf{u} = \lambda \mathbf{u}$ with $\mathbf{u}$ being the fluid velocity. The double Beltrami flow where $\nabla \times \nabla \times \mathbf{u} = \lambda^2 \mathbf{u}$ is also of interest. It has been shown that for a constant λ, the Beltrami flows are non-integrable [2]. Thus, we chose a constant λ in our study.

In this thesis we consider a magnetic field structure similar to a double Beltrami flow, the so-called sine magnetic field [1], and compare our results with a field that

has the same properties as a single Beltrami flow, the Arnold-Beltrami-Childress (ABC) field [8]. We study the spatial diffusion of magnetic field lines and of particles across a wide energy range. We include low energy particles where the magnetic field is approximately constant over the gyro orbit and high energy particles where the field changes significantly over the particle orbit. We begin by considering only the sine field. We characterize the chaotic orbit by the Lyapunov exponents and also characterize diffusion to a scale of 100k orbits. We then treat the sine field as a perturbation to a constant field, and describe the resulting differences in the particle diffusion. Finally, we introduce a simple sinusoidal time variation in the sine field to explore the particle energization effects.

Chapter 2

Sine Magnetic Field

The ABC field is a particular solution of the force-free equation, Eq. 1.1, in Cartesian coordinates . The ABC field takes on the form $\mathbf{B} = (A\sin\lambda z + C\cos\lambda y)\hat{x} + (B\sin\lambda x + A\cos\lambda z)\hat{y} + (A\sin\lambda y + C\cos\lambda x)\hat{z}$ where A, B, C are arbitrary constants and $\hat{x}, \hat{y}, \hat{z}$ are the principle unit vectors. We can normalize the distances by the constant λ, by replacing $(\lambda x, \lambda y, \lambda z)$ with dimensionless (x, y, z) and normalize the magnetic field by a constant magnetic field B_0, and then replacing constants $(A/B_0, B/B_0, C/B_0)$ with (A, B, C). The resulting equation takes on the form similar to the above

$$\mathbf{B} = (A\sin z + C\cos y)\hat{x} + (B\sin x + A\cos z)\hat{y} + (C\sin y + B\cos x)\hat{z} \tag{2.1}$$

The parameters A,B,C are chosen such that $A^2 = 1$, $B^2 = 2/3$, and $C^2 = 1/3$, matching previously studied parameters [8] . Following [11] and [1], we set the cosine terms in the ABC field to zero, and obtain a field with only the sine terms, the sine flow. The resulting field is much different than the full ABC field in terms of the structure of the field lines. The sine field is equivalent to a double Beltrami flow, where $\nabla \times \nabla \times \mathbf{B} = \lambda^2 \mathbf{B}$.

We use the equation

$$\frac{dx}{B_x} = \frac{dy}{B_y} = \frac{dz}{B_z} = \frac{ds}{|\mathbf{B}|} \tag{2.2}$$

to solve for the magnetic field line as a function of the the path length s along the field line.

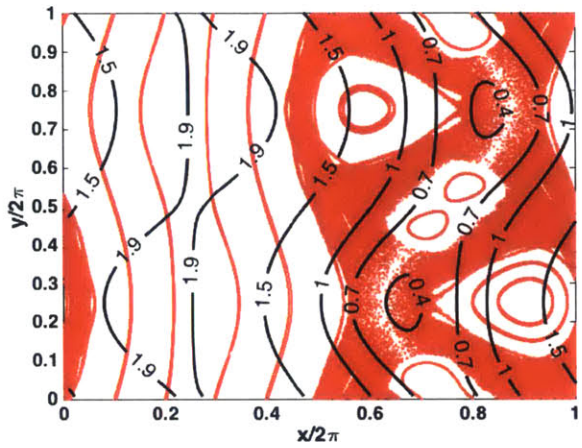

Figure 2-1: Poincaré surface-of-section for $x - y$ plane of ABC flow magnetic field lines, $A^2 = 1$, $B^2 = 2/3$, and $C^2 = 1/3$. The contour lines for $|\mathbf{B}|$ are indicated.

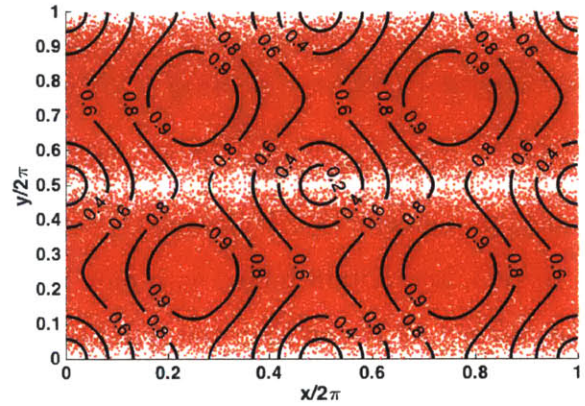

Figure 2-2: Poincaré surface-of-section for $x-y$ plane of sine flow magnetic field lines. The contour lines for $|\mathbf{B}|$ are indicated.

Fig. 2-1 shows the Poincaré surface-of-section at $z = 0$ for ABC magnetic field lines superimposed with the contours of constant magnitude of the field. The plot clearly shows areas of non-chaotic and chaotic field lines. Fig. 2-2 shows the Poincaré surface-of-section at $z = 0$ for magnetic field line of the sine field, superimposed with the contours of constant magnitude of the field. Since the magnetic field is periodic in each spatial dimension with period 2π, we can take the modulus of the spatial variables by the period. The white areas of the section correspond to areas where the field lines are parallel to the $x - y$ plane [8]. The field lines are chaotic over the entire space, unlike the ABC field, which contains islands of non-chaotic field lines. Thus, for any initial condition of a field line, a field line will eventually sample the whole space. Furthermore, even though the field is completely chaotic, the contours of the field magnitude have an unchanging, symmetric, periodic structure. The contours are symmetric about both the x and y axis. These structures seem to manifest themselves in later plots of the asymptotic Lyapunov exponents for particles.

2.1 Lyapunov Exponents for Magnetic Field Lines

To study the non-linear behavior of the the magnetic field lines, we calculate the Lyapunov exponents (LEs) of the field lines These exponents quantify how the field lines diverge from each other in space. In other words, they characterize the linear stability of a small, initial local system. To find these exponents, we linearize the differential equation for the field lines. These equations are the tangent space equations. The resulting solution gives the Lyapunov exponents, one exponent for each dimension of phase space. The largest one characterizes the perturbations on the local system in almost all of the directions in space [4], so we only calculate the largest LE in our exploration.

Furthermore, there are two sets of LEs. The first, the finite-time LEs [13], are calculated after a short evolution, and the second, the asymptotic LEs [10], are calculated over a much longer evolution. The finite-time LEs describe how groups of field lines diverge from a reference trajectory over a relatively short period of time

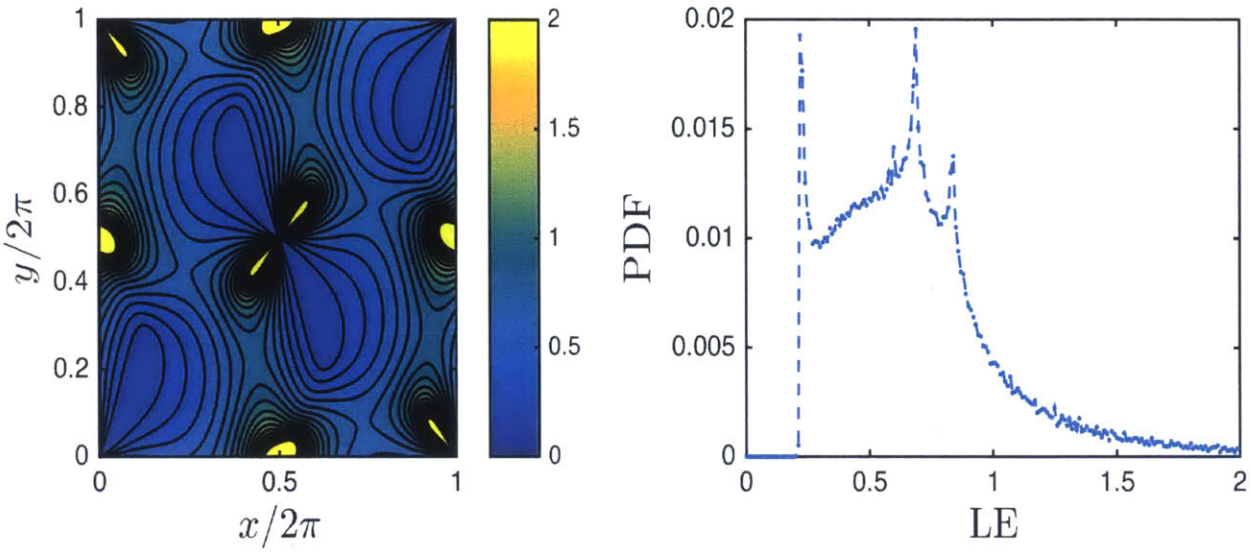

Figure 2-3: Left: FT Lyapunov exponent for magnetic field for a uniform arrangement of 300 by 300 lines, with $x/2\pi$ and $y/2\pi$, for 250 orbits per field line with 2000 steps per orbit. There are several outliers with extremely large exponents. Right: PDF of the LE showing peaks at 0.2 and 0.75.

(such that the linearization remains valid), while the asymptotic LEs characterize the long-term behavior of the perturbations by linearizing the equations, calculating the LE, using Gram-Schmidt orthnormalization, and then repeating.

To study the FT LE of the magnetic field, we start 900 field lines (300 by 300) on an evenly spaced grid over one spatial period $x/2\pi, y/2\pi \in [0, 1]$ in the $x - y$ plane. For the asymptotic LE, we use considerably a less number of field lines because the calculation time is significantly longer than for the FT LE. We start 90 field lines (30 by 30 evenly spaced grid) again in the $x - y$ plane over one spatial period.

In Fig. 2-3 we consider the FT LE. The structure of the contours seen in Fig. 2-2 seems to roughly match the several of the extrema of contours in $|\mathbf{B}|$, with higher magnitude areas of LE ≈ 1 corresponding to lower areas of lower $|\mathbf{B}| \approx 0.3$. Although the similarly between the contours of field magnitude and LE is certainly not exact. This is clear around $x/2\pi = y/2\pi = 0$ for example, as there are both high and low LE areas in similarly shaped $|\mathbf{B}|$ contours. The FT LE contours are also not symmetric across the $x = 0.5/2\pi$ or $y = 0.5/2\pi$ lines.

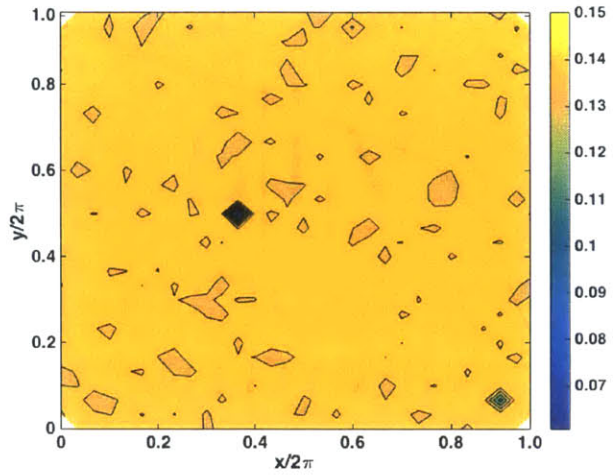

Figure 2-4: Asymptotic Lyapunov exponent for magnetic field with uniform arrangement of 30 by 30 lines, with $x/2\pi$ and $y/2\pi$, for 1,000,000 orbits per field line

We expect the asymptotic LE contours to be much more uniform than in the finite-time case because the field lines eventually lose the memory of the initial conditions due to their chaotic nature, so their long-term behavior should be homogeneous. Fig. 2-4 clearly shows the uniformity (value of approximately 0.14) of the asymptotic LE over the space.

The relative uniformity of aysmptotic LE (≈ 0.14 in magnitude) for the field lines is expected, as the surface of section showed the entire space to be chaotic. There is, however, spatial structure in the FT LE shown by contour plots.

2.2 Spatial Diffusion of Magnetic Field Lines

We also directly explore the long time behavior of the magnetic field. For the magnetic field we chose a reference point r_0 corresponding to a particular field line. We then choose 40 field lines located at positions r_j such that $|r_j - r_0| << 1$ is satisfied and constant, for $j = 1, 2, \ldots 40$, with each field line then uniformly spread around the circle centered around r_0 with radius $|r_j - r_0|$. We choose $r_0 = \mathbf{r}(0) = (0.15, 0.15, 0.1)/2\pi$ and $|r_j - r_0| = 0.01$.

To examine the spatial diffusion of the field lines, we take the ensemble averaged

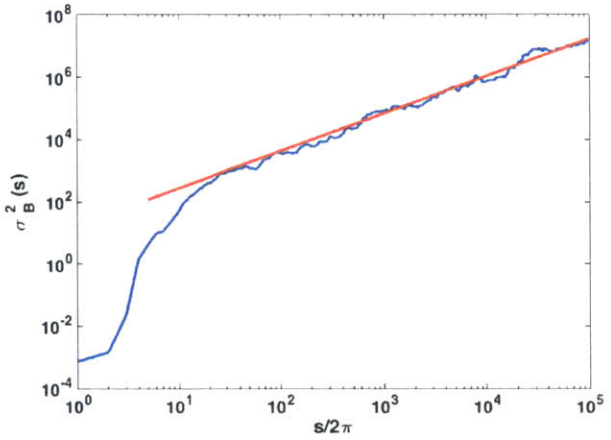

Figure 2-5: Log-log plot of $\sigma_B^2(s)$, the variance, of the distance between 40 field lines from the reference line, as a function of s. The red line shows the least-squares fit to $\sigma_B^2(s)$ over the range $s/2\pi \in [100, 10^5]$. The fit yields $\sigma_B^2(s) = 10^{1.23} s^{1.20}$

separation

$$\mu_B(s) = \frac{1}{N} \sum_{i=1}^{N} |r_i(s) - r_0(s)| \tag{2.3}$$

which is the average distance from the reference line of all the other field lines at a particular s for each field line. We then calculate the variance with respect to the reference field line

$$\sigma_B^2(s) = \frac{1}{N} \sum_{i=1}^{N} (\Delta_i(s) - \mu_B(s))^2 \tag{2.4}$$

where $\Delta_i(s) = |r_i(s) - r_0(s)|$ is the distance between the i-th field line and the reference field line.

Fig. 2-5 shows $\sigma_B^2(s)$ as a function of s. There is an initial interval $s/2\pi \in [0, 10]$ where $\sigma_B^2(s)$ grows quickly. During this interval, the magnetic field lines experience mixing because there is an initial anisotropy. In the remaining interval $s/2\pi \in [10, 10^5]$ the field lines experience diffusion. The linear fit in the final regime results in the power of s equal to 1.2, which indicates that the process is somewhat super diffusive, but still close to normal diffusion. In this regime, the field lines diffuse isotropically, in that the mean separation of the field lines for each coordinate x, y, and z looks similar.

2.3 Charged Particle Motion

Since we consider systems with a low plasma pressure, we can simply study the behavior of particle trajectories, without having to self-consistently evolve a distribution of particles. Single particle tracking, originating from Robert Brown's observation of pollen grain in a fluid, is a useful tool in studying the properties of a system. By using various statistical techniques [18], one can analyze the particle trajectories and characterize the influence of the environment on the particle motion . We have characterized the magnetic field system that the particles move in. It is unclear how that system's behavior then influences the complex particle behavior. In particular, we later calcuate the time averaged mean square displacement (TA MSD) to study the motion.

We describe the trajectories of the particles by the Lorentz equation

$$\begin{aligned} \frac{d\mathbf{r}}{dt} &= \mathbf{v} \\ \frac{d\mathbf{r}}{dt} &= \frac{q}{m}\mathbf{v} \times \mathbf{B}(\mathbf{r}) \end{aligned} \tag{2.5}$$

where $\mathbf{v}$ is the velocity at time t, $\mathbf{r}$ is the position of the particle, q is the charge and m is its mass. The dimensionless equivalent using the parameters above is the equation

$$\begin{aligned} \frac{d\mathbf{r}}{dt} &= \mathbf{v} \\ \frac{d\mathbf{v}}{d\tau} &= \mathbf{v} \times \mathbf{B}(\mathbf{r}) \end{aligned} \tag{2.6}$$

where $\tau = \Omega t, \Omega = qB_0/m$, and $|\mathbf{v}|$ is normalized by $\frac{\Omega}{\lambda}$. We can define the normalized energy of a particle, $E = v^2 = (v_\perp^2 + v_\parallel^2)$ where $v_\perp$ and $v_\parallel$ are the components of the velocity perpendicular and parallel to the direction of the local magnetic field line. Since the magnetic field is not changing with time in the system, the total energy should be conserved. This is ensured by using a symplectic integration algo-

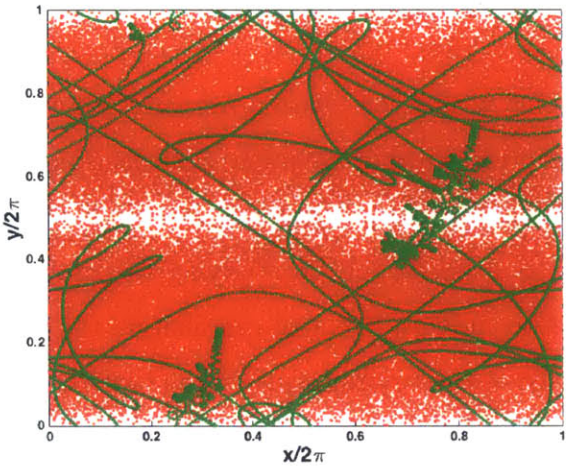

Figure 2-6: Typical chaotic particle trajectory projection onto $x - y$ plane for initial position x/2π=0.995, y/2π=0.477 for 6000 orbits.

rithm. Furthermore, we define a parameter $\xi = \frac{v_{\parallel}}{\sqrt{E}}$, which represents the fraction of the total velocity vector that is parallel to the local field line. That is, if $\xi = 1$, then the velocity is parallel to the local field line, and if $\xi = 0$, the velocity is perpendicular to the local field line.

Fig. 2-6 shows a typical particle trajectory projection overlaid with the field surface of section, for 6000 orbits. For a larger number of steps (on order of $10k$) the projection almost completely covers the plane, suggesting that the particle has sampled the entire space. An interesting feature also shown is the particle 'sticking' to certain locations for short periods of time.

2.4 Lyapunov Exponents for Particle Motion

As a particle moves through space, it is influenced by the local magnetic field line, but is not completely tied to it. The particle can jump field lines, diffusing across them over time. Consequently, we do not expect the values or structure of the LE contours for the field lines to completely match those of the particles. We follow the same procedure for finding the LE as with the field lines, except linearizing Eq. 2.6.

To find the contours for the particle FT LE, we fill one spatial period ($x/2\pi, y/2\pi \in$

$[0, 1]$) uniformly in the $x - y$ plane with an array of 300 by 300 particles all with the same initial conditions in $\sqrt{E}$ and ξ, only differing in position, and then calculate the FT LE for each particle. The FT LE are calculated over 6000 orbits, with 500 steps per orbit. However, there are more parameters that can influence the LE contours for the particles than for the magnetic field lines. The energy and initial orientation (ξ) to the local field line of each particle affect the resulting motion, and thus LE of the particles. To study the affects of ξ on the contours, we chose two different values of ξ: $\xi = 1$ and $\xi = 0$. Because the field lines are chaotic, it is reasonable to assume that an initial orientation with respect to a local field line will not dramatically change the particle asymptotic LE, as the information eventually is lost. For some parameters this is true. However, some initial conditions, like higher energies, do result in a different spatial structure.

To examine the effects of energy on the contours, we choose four different values of $\sqrt{E}$, each increasing by an order of magnitude: $\sqrt{E} = 0.01, 0.1, 1.0$, and 10.0. Fig. 2-7 summarizes these results. For small energies, the time step of 500 steps/orbit is sufficiently small compared to the particle gyrofrequency, so that the orbit is resolved. For the larger energies considered, it is possible that this resolution is not sufficient. However, for the largest energy, $\sqrt{E} = 10$, even doubling the resolution to 1000 steps/orbit and then doubling again to 2000 steps/orbit did not significantly change the contour plots of FT and asymptotic LE for several representative runs. So the time step used for all of the LE calculations is sufficient to resolve the motion. For brevity, we present the contour plots for $\xi = 0$. The contour plots for $\xi = 1$ are mostly similar and it is noted when they are not.

For $\sqrt{E} = 0.01$ the FT LE is relatively uniform in certain areas across the space with a value around 0.06. The other non-uniform areas have a vortex-like structure with many small and closely spaced contours. It is clear that the contours are similar to the $|\mathbf{B}|$ contours in Fig. 2.1. The location of the areas with non-uniform FT LE closely corresponds relatively closely to the areas of low $|\mathbf{B}|$ contours, where the normalized magnetic field strength was about 0.2 (around three times lower than the surrounding areas). The areas of more uniform LE lie around the local maximum

($|\mathbf{B}| > 0.8$) and saddle points of the $|\mathbf{B}|$ contours. Looking closer at the non-uniform regions reveals small areas with much higher FT LE than the surrounding particles. These small areas could correspond to the LE values calculated from a few or even a single particle. A similar contour structure results from $\xi = 1$, with the initial particle velocity parallel to the local field line. In this case, the initial orientation of the velocity with respect to the local field line does not seem to matter. This is expected because the particles eventually lose memory of the initial condition. The structure of the contours changes slightly when the energy is increased by an order of magnitude to $\sqrt{E} = 0.1$. Most of the space has a FT LE of about 0.04, but there are now significantly larger areas with LE below 0.02. However, for even larger energies, the exponents across the space are no longer as uniform. For example, for $\sqrt{E} = 1$ (three orders of magnitude larger than in the first plot) a large portion of the space has an exponent of about 0.25 and is not uniform.

The initial orientation of the velocity ξ also changes the contour plot. For $\xi = 0$, the structure becomes non-uniform and similar values compared with $\xi = 1$ were found, although the structure between them was different. For $\sqrt{E} = 10$ the structure of the contours changes significantly. The LE are mostly around 0.15 (similar to previous plots), but there are areas of the space where the LE are failed to compute properly, most likely due to the large energy. The contours for $\sqrt{E} = 10$ and $\xi = 1$ have similar values, but different structure. Interestingly, the contour plots for $\sqrt{E} = 10$, are similar to their counterpart plots with the asymptotic LE.

Fig. 2-8 summarizes the results for the asymptotic LE. For the asymptotic LE we see much more uniformity in the values across the space. For $\sqrt{E} = 0.01$, the LE is small at about 10^{-4}, but non-zero, for most of the space. In the figure, we plot the log of the LE, to better show the results. For $\sqrt{E} = 0.1$, we see that the LE remains relatively uniform, but has grown in magnitude compared to the smaller energy results. For larger energies with begin to see results that match the FT LE. For $\sqrt{E} = 1.0$ the peak in the asymptotic PDF is around 0.23, at the same location for the FT LE. The only difference is a larger spread for the FT LE. At $\sqrt{E} = 10.0$, the asymptotic LE and FT LE have a very similar structure. It is possible that this

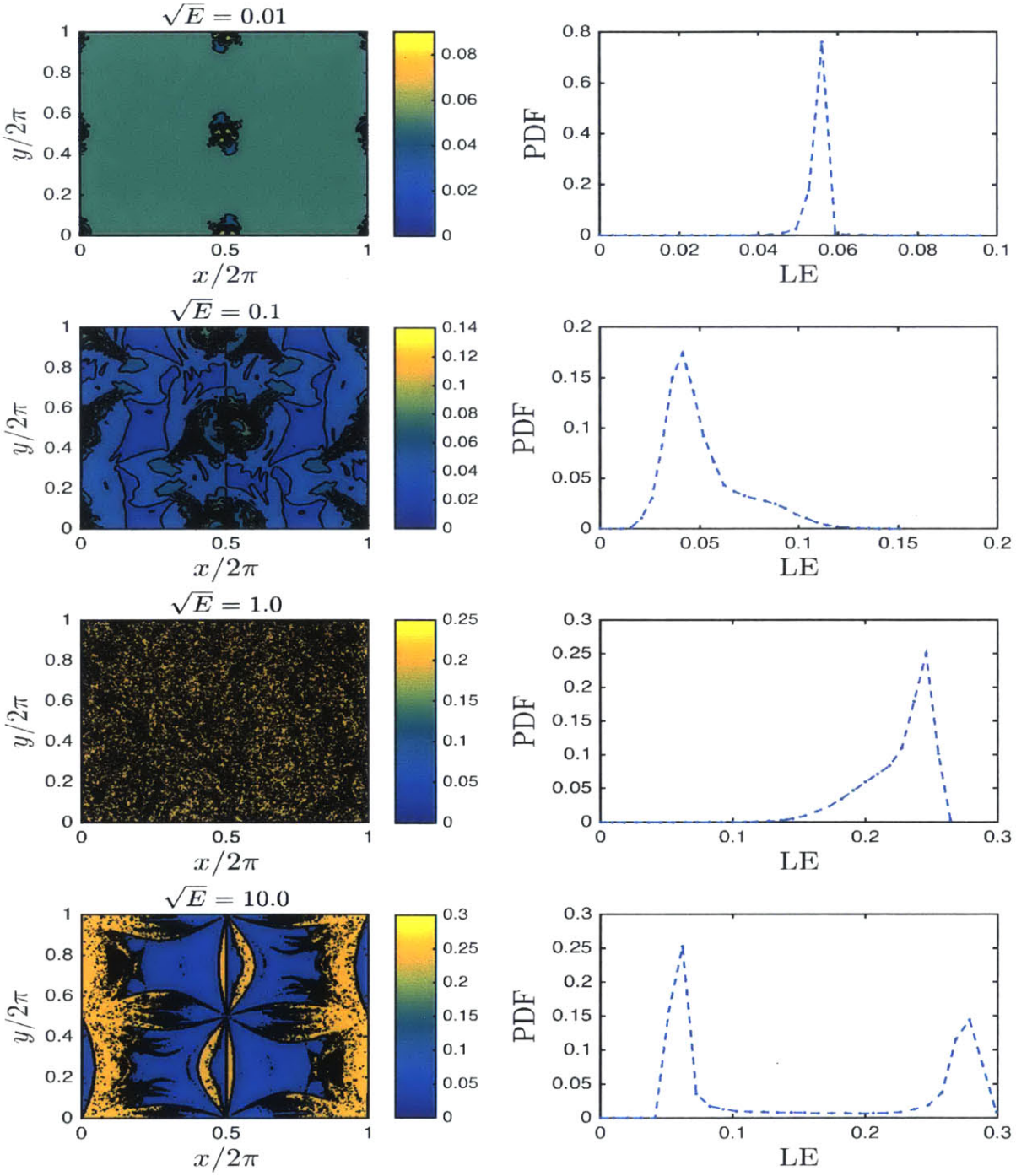

Figure 2-7: Spatial distribution and PDF of the particle FT LE and for varying energies, and $\xi = 0$.

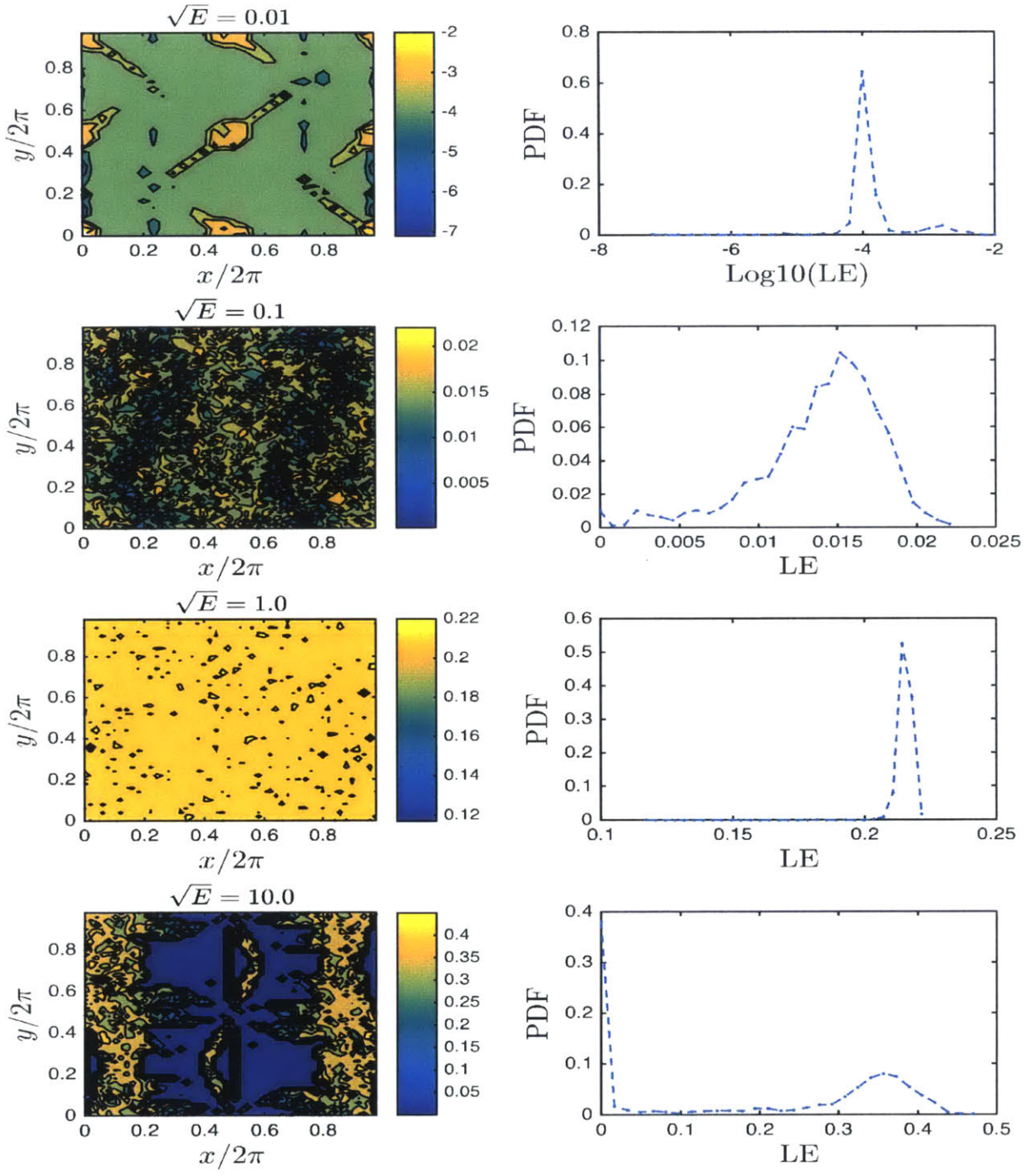

Figure 2-8: Spatial distribution and PDF of the particle asymptotic LE and for varying energies, and $\xi = 0$.

similarity at larger energies is caused by the larger energy particles exploring a large portion of the phase space even in the short calculation time for the FT LE, so it effectively matches the asymptotic result.

2.5 Diffusion

For the particles we calculate the time averaged mean square displacement (TA MSD) and then ensemble average: [12]

$$\langle\overline{\delta^2}\rangle = \frac{1}{N_p}\sum_{p=1}^{N_p}(\frac{1}{N-k}\sum_{i=1}^{N-k}((r)_{i+k}^{(p)} - \mathbf{r}_i^{(p)})^2) \tag{2.7}$$

where N_p is the total number of particles, N is the total number of orbits, and $k = 0, 1, 2, \ldots, K$ with $K < N$. The outer sum represents the ensemble average and the inner sum represents the mean square displacement for data points separated by time $\Delta t = k\delta t$. In many cases, like Brownian motion, in the limit of infinite time a single particle TA MSD approaches the ensemble-averaged, mean-squared displacement [18]:

$$\langle r^2(t)\rangle = \int_0^\infty r^2 P(r,t)dV = 2dK_b t^b \tag{2.8}$$

where P(r,t) is the particle probability density at a given radial distance and time, d is the dimension of the isotropic system, and K_b is the diffusion coefficient. Such systems are ergodic. For non-ergodic systems, the individual particle TA MSD themselves become random variables. This behavior is discussed later.

We take a similar power-law form as Eq. 2.8, defining the MSD in terms of linear parameters a and b in log-log form

$$\log(\langle\overline{\delta^2}\rangle) = \log(a) + b\log(\Delta t) \tag{2.9}$$

The parameter a is connected to the diffusion coefficient by $10^a = 2dK_b$. The parameter b indicates the type of motion that the particles undergo [15]. $b = 1$ and $b =$

2 correspond to normal diffusion and ballistic trajectories respectively. Anomalous diffusion is characterized by subdiffusion with $b < 1$ or superdiffusion $1 < b < 2$. In summary, for ballistic motion, $\langle\overline{\delta^2}\rangle \sim t^2$, for normal diffusion (i.e. random walk), $\langle\overline{\delta^2}\rangle \sim t$, and for a sub diffusive process, the power dependence is lower than 1.

[16] found that in the ABC field for a low energy particle, $\langle\overline{\delta^2}\rangle$ contains several regimes. For example, for $\sqrt{E} = 0.01$, there are three regimes, corresponding to one ballistic, one mixing, and one superdiffusive region. The first balistic regime is very short and quickly moves into the intermediate mixing regime. The $\langle\overline{\delta^2}\rangle$ then settles into a long time scale superdiffusive regime. We focus on this final regime that characterizes the long term diffusive properties of the ensemble. For particles in the ABC field, the power law time dependence of the TA MSD goes like $b = 1.575, 1.72$ for $\sqrt{E} = 0.01, 0.1$ respectively, and the corresponding values for the sine field are $b = 1.24, 1.068$. Increasing the particle energy in the ABC could produce additional effects due to the presence of chaotic and non-chaotic regions of magnetic field lines. These particles can drift out of the chaotic region and possibly become trapped in the regular region. In the sine field however, the entire region is chaotic, so we take a much larger energy range. Furthermore, we only consider the mean square displacement along the $x - y$ plane, since this cross field diffusion becomes important when we add a constant background field on top of the sine field. In Eq. 2.8, this means using $\mathbf{r}^2 = x^2 + y^2$. Since the sine field is isotropic, taking the mean square displacement along a plane corresponds to removing one dimension from the system. The dimension only effects the numerical factor a and not the exponent b as in Eq. (2.8), so we have not changed the quantities we are comparing. We compared the b exponent for several runs taking $x - y$ or full TA MSD and found that it remained the same.

We initially take different orders of magnitude of energy, summarized in Table 2.1. Most notably, the low energy particle diffusion is much closer to normal diffusion than in the ABC field. However, we see a clear transition into ballistic motion for $\sqrt{E} = 10.0$. This transition can be understood as the gyroradius exceeding the length scale of the magnetic field $L \approx 2\pi$. In normalized units the gyroradius is

Table 2.1: Parameters found for Eq. 2.9. The ABC data is from [16]

	Sine			Sine + Bo			ABC		
$\sqrt{E}$	Onset	a	b	Onset	a	b	Onset	a	b
0.01	10^2	-1.02	1.24	10^3	-7.51	1.99	10^2	-3.613	1.575
0.1	10^3	0.4328	1.068	10^2	-5.69	1.95	10^1	-2.0	1.65
1.0	10^1	2.072	0.9852	10^2	-4.70	1.99			
10.0	10^0	4.073	1.891	10^0	0.067	1.55			

simply $R = v_\perp/B$. Since $v_\perp$ and B vary, we pick their maximum values to give a characteristic lengthscale. For the sine field $B_{max} = 2.0$ and the maximum $v_\perp = \sqrt{E}$ occurs when $\xi = 0$, when the particles initial velocity is completely perpendicular to the local field line, so $R_{max} = \sqrt{E}/B_{max}$. For $\sqrt{E} = 1.0, R_{max} = 0.5$ is still well below L, while for $\sqrt{E} = 10.0, R_{max} = 5$, is on the order of L. In fact as Fig. 2-13 shows for $E = 1.0$ we can scale down the sine field by a factor of 10 so that its R_{max} is the same as $E = 10.0$ and see that the mean square displacement behavior for the larger energy is recovered. This simple result shows that if we scale B_{max} and $\sqrt{E}$ such that R_{max} is constant, the results do not change. The particle TA MSD behaves linearly in R_{max}. In other words, there is a self-similarity in that no matter what scale we look at, the phenomena remains the same.

In general though, not all the individual particles exhibit the same behavior in the large time limit. This behavior is known as ergodicity breaking. The probability distribution of the particle displacement for example, can have 'fat' tails, in that the higher order moments diverge to infinity. Ergodicity breaking suggests the entire phase space is not accessible to all particles. In an ensemble of particles, some particles will reach regions that others will never reach, even in infinite time. As a result, the individual TA MSD can show vastly different behavior, and when averaged, will not converge to a single MSD described in Eq. 2.8, as expected by Brownian motion for example. [5] noted that for a phase space without (a priori) inaccessible regions, as this system is, it is useful to consider 'weak' ergodicity breaking. There are local regions in phase space where particles may become trapped or experience some other anomalous behavior, but no strict barriers are present; given enough time, the particles can continue diffusing and exploring the phase space. We will quantify the

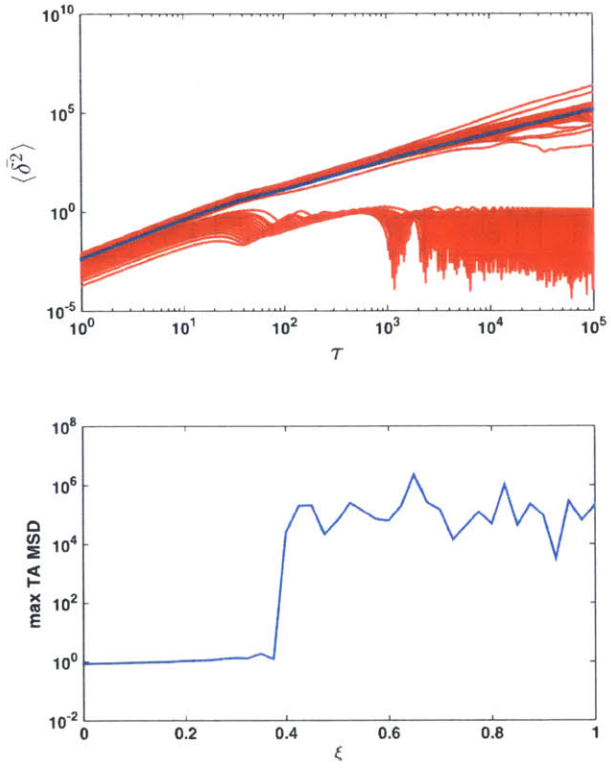

Figure 2-9: The top plot is the TA MSD for the sine field at $\sqrt{E} = 0.01$: $\langle\bar{\delta}^2\rangle$ in blue, the individual $\bar{\delta}^2$ are in red. The bottom plot shows the max($\langle\bar{\delta}^2\rangle$) as a function of ξ to help identify which particles are which in the top plot.

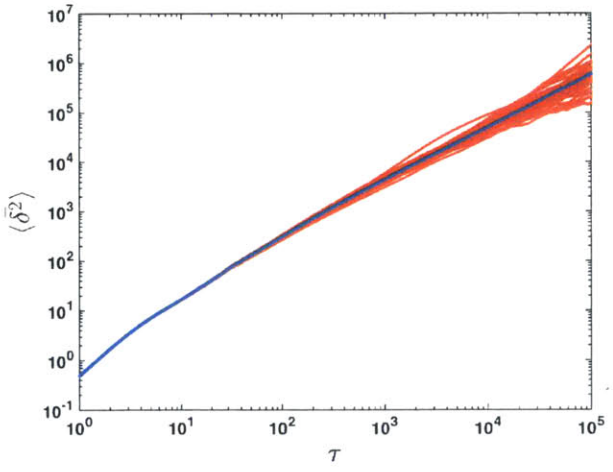

Figure 2-10: TA MSD for the sine field at $\sqrt{E} = 0.1$: $\langle\bar{\delta}^2\rangle$ in blue, the individual $\bar{\delta}^2$ are in red.

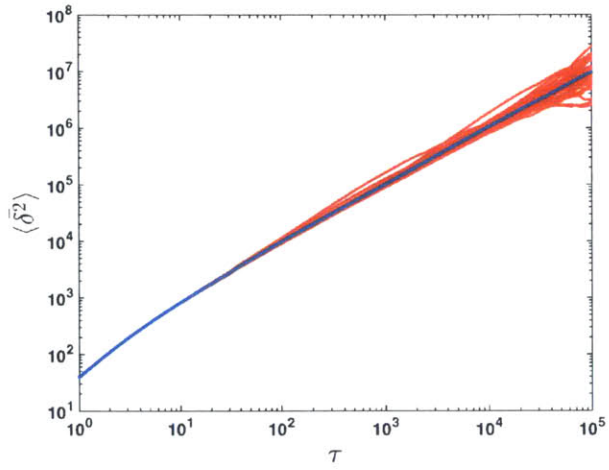

Figure 2-11: TA MSD for the sine field at $\sqrt{E} = 1.0$: $\langle\bar{\delta}^2\rangle$ in blue, the individual $\bar{\delta}^2$ are in red.

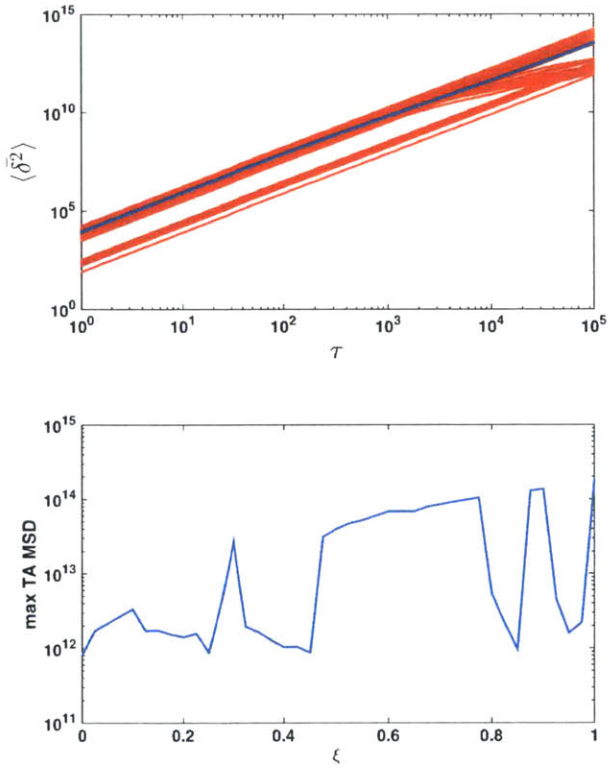

Figure 2-12: The top plot is the TA MSD for the sine field at $\sqrt{E} = 0.01$: $\langle\bar{\delta}^2\rangle$ in blue, the individual $\bar{\delta}^2$ are in red. The bottom plot shows the max($\langle\bar{\delta}^2\rangle$) as a function of ξ

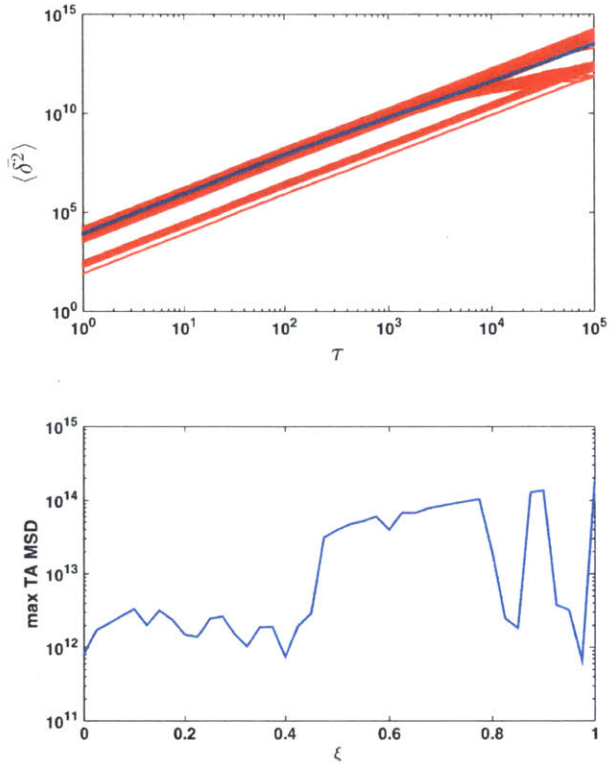

Figure 2-13: Same as Fig. 2-11 with sine field divided by factor of 10, and the bottom plot shows the max($\langle \tilde{\delta}^2 \rangle$) as a function of ξ. Note the similarity to Fig. 2-12

ergodicity breaking later with the ergodicity breaking parameter EB.

Fig. 2-9, 2-10, 2-11, 2-12 show the individual mean square displacements in red and the ensemble average in blue. When there is a large spread in the ensemble of TA MSD, we also plot the maximum TA MSD value (typically the value at the largest time scale) against ξ. This allows an easy identification of which particles belong to which TA MSD trajectories. For $\sqrt{E} = 0.01$, roughly half of the particles (those with $\xi < 0.4$) have a MSD that saturates at time scales of 100 orbits, and the other half (those with $\xi > 0.4$) have MSD with $b = 1.24$, the value in the ensemble average. For the other energies there is much less of a difference between the individual mean square displacements. This difference can be quantified by the ergodicity breaking parameter EB [12] [17], the variance of $\overline{\delta^2}$ defined

$$\mathrm{EB} = \frac{(\langle(\overline{\delta^2})^2\rangle - \langle\overline{\delta^2}\rangle^2)}{\langle\overline{\delta^2}\rangle^2} \tag{2.10}$$

If the system is ergodic, when the individual particle $\overline{\delta^2}$ all converge large time limit $\Delta t \to \infty$, then $EB = 0$, the classic example being Brownian motion. If we have an ensemble of particles undergoing Brownian motion, and calculate their individual $\overline{\delta^2}$, initially there will be differences among them due to initial conditions, even if the ensemble average shows Brownian motion. Eventually the individual TA MSD will converge to the ensemble average, and the spread will go to 0. Another similar example is the Continuous Time Random Walk (CTRW) model. Instead of solely the direction of a random walker being random after a set spatial and temporal step, the CTRW model has a particle executing a random walk with both the step size and time step as random variables. Based on the parameter choices, there can be different diffusion effects [18] [3]. If the step sizes are relatively small, then the system is essential the same as the standard random walk, with normal diffusion and $EB = 0$. However, other combinations can yield sub-diffusion or superdiffusion, and also leads to $EB \neq 0$. For some of these cases, $EB \sim 0.1 - 0.5$ [6], showing only weak ergodicity breaking.

We also further explore the parameter space by plotting the maximum $x - y$

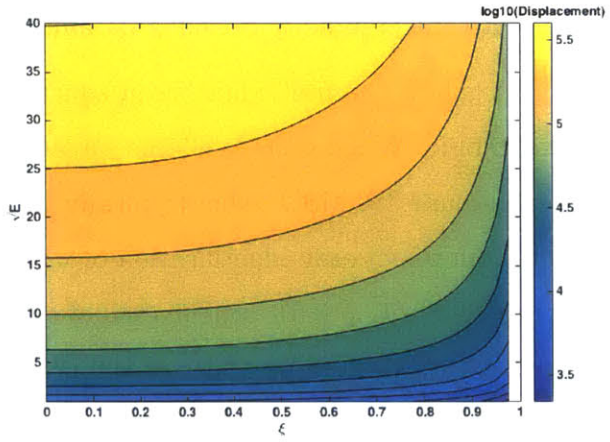

Figure 2-14: Max $x - y$ displacement for free particles $d_{XY} = \sqrt{1-\xi^2}\sqrt{E}T$ at $T = 10k$ plotted for $\sqrt{E}$ vs. ξ.

displacement $d_{xy} = \max(\Delta r_{xy}[1 : \mathrm{T}])$ where T is the maximum orbit considered, for a range $\sqrt{E} \in [1.0, 40.0]$ vs. ξ. For comparison, Fig. 2-14 shows the resulting $x - y$ displacement for a free particle, as in a particle that moves at a constant velocity for all time. The $x - y$ displacement is simply $d_{XY} = \sqrt{1-\xi^2}\sqrt{E}T$: larger energy particles go farther in the $x - y$ plane, but particles with ξ close to 1 have most of that energy in the z direction. If the energy scaling is introduced into T, the energy dependence drops out: the displacement is purely a function of the angle.

Fig. 2-16 shows the d_{xy} for particles in the sine field. Changing the max orbit T evolves the plot in time and allows us to verify any features that persist over time, and are not simply present at a particular time. Since running up to 300k orbits is computationally expensive, we instead chose to take up to 10k orbits. We can also eliminate the expected simple energy dependence on displacement by using $T = T_{norm} = 10k/\sqrt{E}$, scaled inversely by the energy. So with this T normalization we calculate the max displacement for $\sqrt{E} = 1.0$ up to 10k orbits, but up to 250 orbits for $\sqrt{E} = 40$.

The previous discussion of the ensemble averages for the mean square displacement reveals a clear dependence on the longer term particle behavior on $\sqrt{E}$ and to a lesser extent ξ. Fig. 2-16 shows large scale structure in the parameter space. There is a relatively uniform behavior in particle motion at $\sqrt{E} > 10.0$ and $\xi > 0.2$. Particles

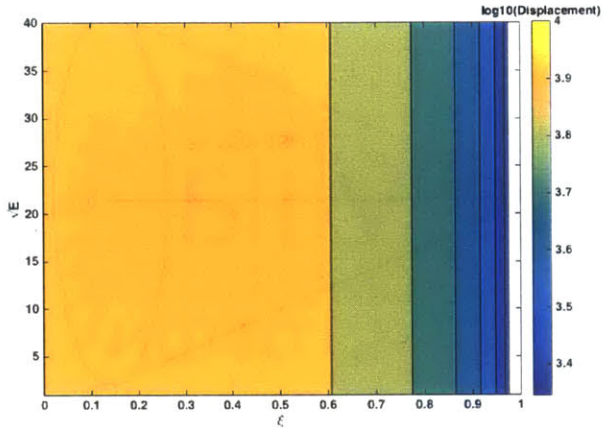

Figure 2-15: Max $x - y$ displacement for free particles at $T = 10k/\sqrt{E}$ plotted for $\sqrt{E}$ vs. ξ.

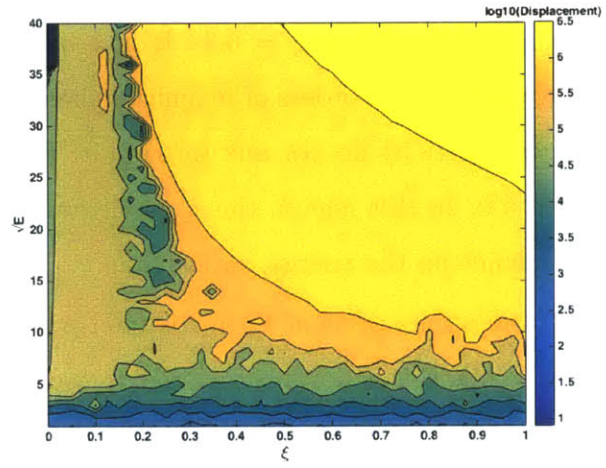

Figure 2-16: Max $x - y$ displacement for particles in the sine field at $T = 10k$ plotted for $\sqrt{E}$ vs. ξ.

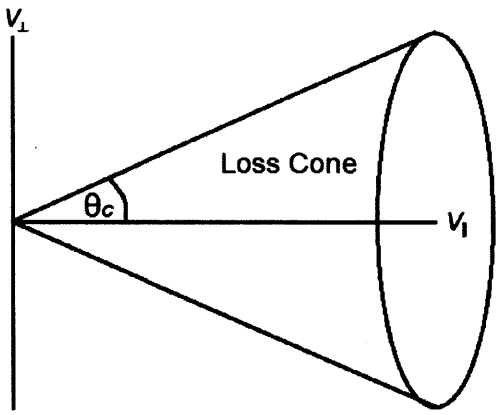

Figure 2-17: Diagram of a loss cone in velocity space, showing the critial angle θ_c.

in this region have the greatest amoutn of displacement. If we instead use T_{norm}, we find that the contours in this large, uniform region become vertical, roughly matching the normalized free particle result. However, in this region the $x - y$ displacement increases with ξ, which is the opposite to the free particle case. There is also a distinct region of comparable energy, but lower ξ. Particle displacment in this region is similarly uniform, but is an order of magnitude lower. Additionally, a 'barrier' region separates these two previous uniform regions. This region is approximately independent of energy and is located at $\xi = 0.2$. It is a barrier in the sense that particles in this strip have almost two orders of magnitude less displacement, and the nearby higher displacement particles do not mix through it. Finally, there is a lower energy region with $\sqrt{E} < 5.0$. In this region, the d_{xy} contours are mostly horizontal, indicating a larger dependence on the energy, rather than ξ.

We evolved the plot from a max orbit of 1k to 10k, and saw that features like the barrier structure remain. While this is not a large range to evolve the plot through, it does eliminate the possibility that the snapshot of displacement at $T = 10k$ is simply a random fluctuation, whereby at other T the plot would appear radically different.

The barrier structure gives some insight into the behavior of the particle motion. Particles to the right in ξ, with higher initial motion along the local field line, move more freely than particles on the left, with higher initial perpendicular motion relative to the local field. Additionally, the barrier is approximately independent of $\sqrt{E}$.

These characteristics indicate possible loss-cone behavior, in a magnetic mirror-like system. Particles moving in a region with a magnetic field gradient will gyrate and stream along a magnetic field line starting at an initial magnetic field magnitude $\mathbf{B} = \mathbf{B}_{min}$ until it hits a value $\mathbf{B} = \mathbf{B}_{max}$, at which it will stop and reverse direction, before finally passing through its starting location in the opposite direction. This motion completely depends on the initial angle of the particle's velocity with respect to the magnetic field line (as long as the Larmor radius is small compared to the length scale of the gradient, of course). If the angle is too small, the particle will not become trapped and will escape. This loss cone is typically defined in terms of a critical angle shown in Fig. 2-17 where $\sin(\theta_c) = \sqrt{B_{min}/B_{max}}$ [7]. Particles with angles $\theta < \theta_c$ or equivalently $\xi > \xi_c$ will escape the magnetic mirror. In our notation, we have

$$\sin(\theta) = v_\perp/\sqrt{E} = \sqrt{1-\xi} \tag{2.11}$$

independent of the energy. Looking at Fig. 2-16 we see that this is the case for high energy, with $\xi_c \approx 0.2$ or $\theta_c \approx 78.5°$. In the free particle plot, particles with the largest energy and smallest ξ have the greatest d_{xy}. In contrast though, in the sine field, those with the largest energy and ξ have the greatest d_{xy}, in agreement with the loss cone behavior, even though we only considered the $x-y$ displacement. However, for lower energies $\sqrt{E} < 10$ the cutoff disappears and the contours no longer depend strongly on ξ.

Chapter 3

Sine Field Superimposed on a Background Magnetic Field

We now add a background field $B_0 = 5.0$ along the z direction onto the static sine field, effectively treating the sine field as a perturbation. Without the perturbation, the particles exhibit no diffusion across the field. There is gyromotion perpendicular to the field and free streaming parallel to the field. The perturbation introduces the effect of cross field diffusion.

For a simpler system studied in [15] with a constant field in the z direction superimposed with an axially varying field in the x direction it is possible to derive analytic results for the cross field diffusion. They found that the magnetic field lines diffuse in the perpendicular plane according to normal diffusion and that the particles experience subdiffusion with the exponent $b = 1/2$. This is attributed to the idea that the particles remain tied to the magnetic field lines, which diffuse perpendicularly; in general, the particles do not diffuse separately from the field lines. In our system though for the particles, we find superdiffusion across the field for the ensemble of particles.

3.1 Relative Scaling of the Sine Field with Respect to The Constant Field

As done previously with the sine field, we explore the effects of scaling the sine field on the particle mean square displacement. We first scale the entire magnetic field, including the constant field, by a constant α:

$$\mathbf{B} = \alpha(B_{sine} + B_o) \tag{3.1}$$

If we divide the entire B by a factor of 10, $\alpha = 1/10$, for particles with $\sqrt{E} = 1.0$ we obtain a power law MSD with $b = 1.1$, which does not match the $\sqrt{E} = 10.0$ result of $b = 1.55$ expected for completely linear scaling. Thus, we find that unlike the pure sine field, the system does not scale linearly in $R_{max} = \sqrt{E}/B_{max}$.

Furthermore, we scale only the sine field, leaving the constant field at $B = 5.0$.

$$\mathbf{B} = \alpha(B_{sine}) + B_o \tag{3.2}$$

This allows us to identify different behaviors that the sine field introduces in conjunction with a background field. We focus on $\sqrt{E} = 1.0$ and look at the ensemble average results. A more detailed discussion of the actual ensemble is presented later in the section, as the average is sometimes heavily skewed by outliers.

Fig. 3-1 shows the mean square displacement for the full field (background + sine field) and for the perturbations for $\alpha = 1/2$, $1/4$, $1/6$, $1/8$, and $1/10$. The labeling is such that $\alpha = 1/2$ corresponds to $d2$, $\alpha = 1/4$ corresponds to $d4$, and so on. From a first look, we would expect a progression tending to the constant field results. As expected, reducing the perturbation size causes the system to saturate. Even with a factor of 10 reduction though, the particles still experience diffusion. Without any perturbation, the mean square displacement lies $\sim 10^{-15}$, as the particles are completely confined. Even scalings of $\alpha \approx 1/100$ do not reach those magnitudes. This result shows that the sine field, even if present at a small scale, will cause cross field diffusion. What changes is the saturation timescale. Regardless of the size of the

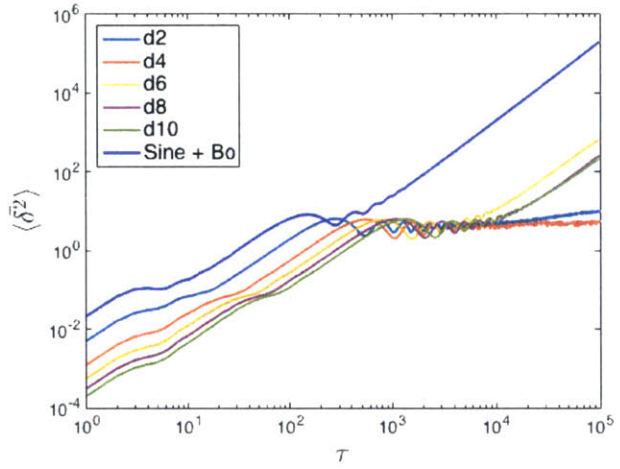

Figure 3-1: TA MSD for Sine + Bo, and for the Sine field scaled down by a constant factor labeled with the letter 'd'.

perturbation, the TA MSD saturates once it reaches $\sim 10^0$. The perturbation size also roughly determines the time scale at which particle spends in the saturated region. For the full perturbation, saturation only occurs near $\tau \approx 10^2 - 10^3$ and shortly afterwards the particle ensemble continues to diffuse (in this case with $b = 1.99$). When the perturbations are scaled down, the TA MSD saturates for many order of magnitudes in τ. Fig. 3-1 shows that some of these long time scale saturations eventually begin to diffuse, but only after an order of magnitude in τ.

We also scale up the perturbations in Fig. 3-2, multiplying by an overall factors of $\alpha = 2, 4, 6, 8,$ and 10. The notation is such that $\alpha = 2$ corresponds to $m2$ and so on. The sine field 'perturbations' are no longer such, as the multiplicative scaling quickly moves the sine field magnitude on the order of $B_o = 5.0$. For example, with $\alpha = 2$ the maximum sine field magnitude B_{max}^{sine} increases from 2.0 to 4.0, and then to 8.0 for $\alpha = 4$. In principle though, we should recover the pure sine field results discussed in the previous section, as the sine field begins to completely dominate, and the constant field turns into the perturbation. Comparing with the $\alpha = 2$ MSD, it is clear that the saturation region at $\langle\overline{\delta^2}\rangle = 10^0$ completely disappears: the particle ensemble moves straight into a diffusive regime. Using finer scalings, the saturation disappears at a scaling of about 1.75, where B_{max}^{sine} is about 70 percent of the background field,

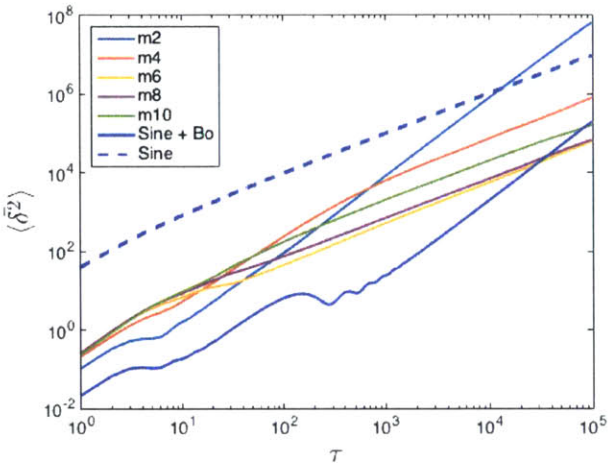

Figure 3-2: TA MSD for Sine + Bo, pure Sine, and for the Sine field scaled up by a constant factor labeled with the letter 'm'

compared to the original 40 percent.

Interestingly, although the saturation region disappears, the slope b remains the same between these two cases, $\alpha = 1$ and $\alpha = 2$. This indicates that the constant field still affects the diffusive properties of the ensemble for small scalings of $\alpha > 1$. With any larger α than 3, the constant field effects are removed, as the slope b follows the result for the pure sine field, which is normal diffusion. Of course, the factor a in the TA MSD does not match between them, as the field magnitudes are no longer the same. For $\alpha = 3$, there is an intermediate regime with $b \approx 2$, but eventually turns to normal diffusion. In fact, the maximum magnetic field magnitude at $\alpha = 2$ and 3 become on the order of the constant field, $B_{max}^{sine} = 4$ and 6 respectively.

3.2 Diffusion

Table 2.1 summarizes the ensemble averaged mean square displacement over the previously discussed four order of magnitude $\sqrt{E}$ range. Fig. 3-3, 3-4, 3-5, and 3-6 show the individual mean square displacements in red and the ensemble average in blue.

We also explore larger energies, which have maximum Larmor radii R_{max} (in this case dominated by the constant magnetic field contribution) approaching the

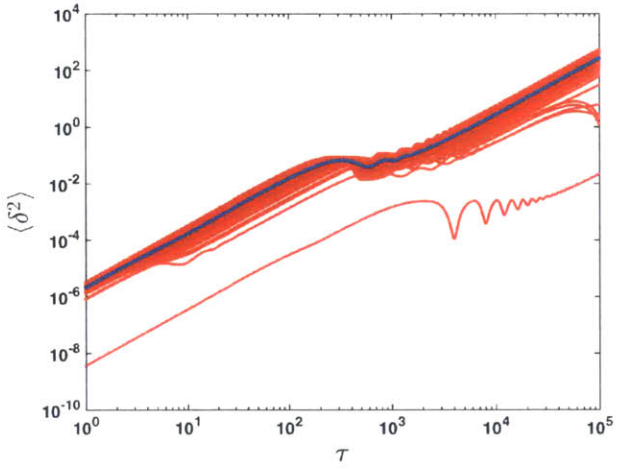

Figure 3-3: TA MSD for the sine+Bo field at $\sqrt{E} = 0.01$: $\langle \bar{\delta}^2 \rangle$ in blue, the individual $\bar{\delta}^2$ are in red. The bottom plot shows the max($\langle \bar{\delta}^2 \rangle$) as a function of ξ

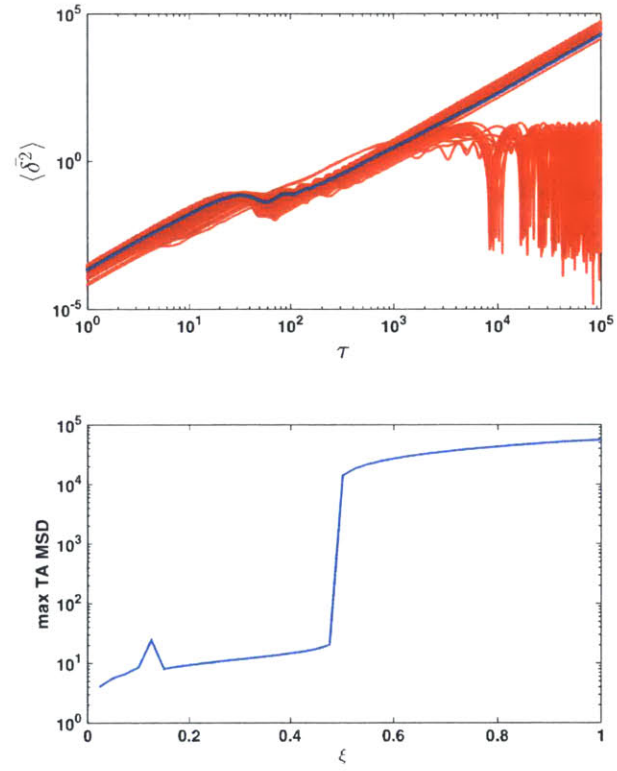

Figure 3-4: The top plot is the TA MSD for the sine+Bo at $\sqrt{E} = 0.1$: $\langle \bar{\delta}^2 \rangle$ in blue, the individual $\bar{\delta}^2$ are in red. The bottom plot shows the max($\langle \bar{\delta}^2 \rangle$) as a function of ξ

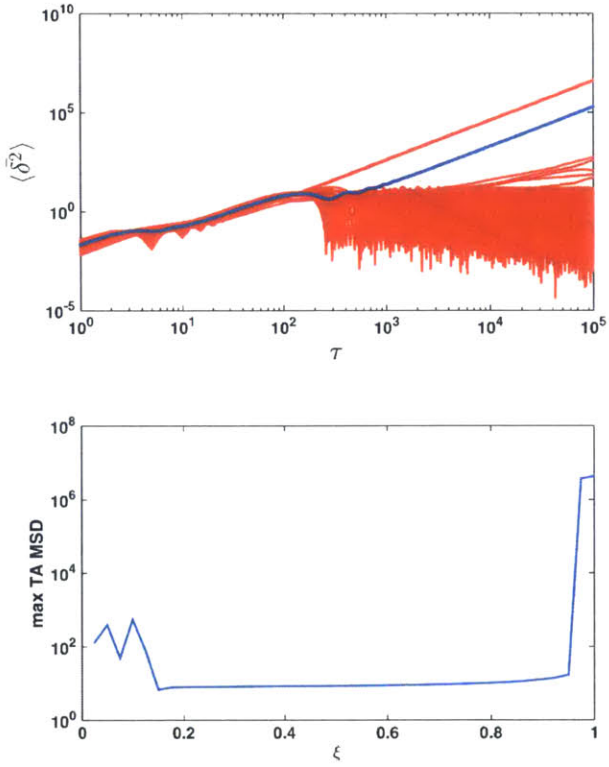

Figure 3-5: The top plot is the TA MSD for the sine+Bo field at $\sqrt{E} = 1.0$: $\langle\bar{\delta}^2\rangle$ in blue, the individual $\bar{\delta}^2$ are in red. The bottom plot shows the max($\langle\bar{\delta}^2\rangle$) as a function of ξ

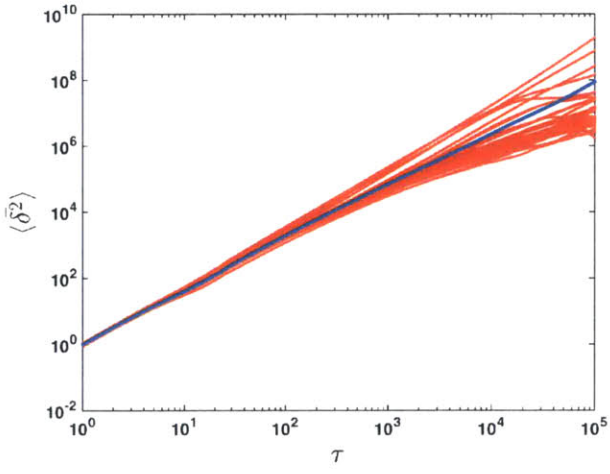

Figure 3-6: TA MSD for the sine field at $\sqrt{E} = 10.0$: $\langle\bar{\delta}^2\rangle$ in blue, the individual $\bar{\delta}^2$ are in red.

perturbation scale length of 2π; for example, if we consider only the constant field magnitude with $B_{max} \approx 5.0$, for $\sqrt{E} = 40$, we have $R_{max} = 8.0$, or with the sine field contribution $B_{max} \approx 7.0$ we have $R_{max} = 5.7$. In Fig. (3-7) we plot the maximum $x - y$ displacement on the same $\sqrt{E}$ and ξ range as in Fig. 2-16, but at a maximum orbit $T = 300k$, instead of $T = 10k$ as before.

There are clear structures found in this parameter space that are quite different than with the pure sine field: there are rough bands of alternating very high and low displacement, of high $\sqrt{E}$ and ξ, and regions of that are much more uniform, but still have some banding structure. By evolving the plot from $T = 10k$ to $T = 300k$, we confirm that the structures persist over long times.

It is clear that the ensemble changes behavior significantly at around zz$\sqrt{E} \approx 25.0$. Because of the complexity of the field, we can examine three possibly relevant length scale parameters, R_{max} as used before, R_{min}, and R_{avg}. R_{min} and R_{avg} take the same form as R_{max}, except with B_{max} replaced with the minimum and average total B magnitude, respectively. In the case of R_{min}, the sine field contributes negatively, so $B_{min} = -2.0 + 5.0 = 3.0$. Since the sine field fluctuates symmetrically between negative and positive values, we have $B_{avg} = 5.0$. At $\sqrt{E} = 25.0$, $R_{max} = 3.57$, $R_{min} = 8.33$, and $R_{avg} = 5.0$. Interestingly, R_{min} exceeds the magnetic field scale length. If R_{min} is an important criterion in the parameter space then we expect the energy at which $R_{min} \approx 2\pi$ to exhibit transition-like properties. This energy corresponds to $\sqrt{E} \approx 19$. A transition remains plausible looking at the displacment in Fig. 3-7.

This shift in behavior is also apparent in the top part of Fig. 3-8 where we plot the power law exponent b of the diffusive regime in $\langle \bar{\delta}^2 \rangle$. For $\sqrt{E} < 25.0$ there is a large variability from ballistic motion $b = 2.0$ all the way down to normal diffusion $b = 1.0$. For example, for $\sqrt{E} = 1.0$ we see ballistic motion, but for $\sqrt{E} = 3.0$, b drops to 1.2, and then at $\sqrt{E} = 5.0$ there is normal diffusion. This variability might indicate that at these energies the outlier's effects are particularly significant. After $\sqrt{E} = 25.0$, the b profile becomes much flatter and uniform with a value of $b \approx 1.8$, greatly contrasting the profile of the lower energies. The previous hypothesis of a

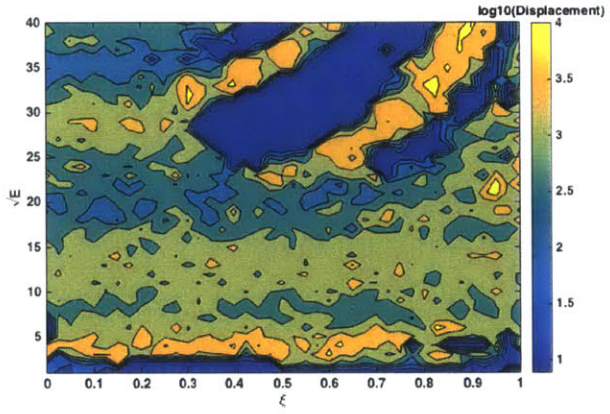

Figure 3-7: Max $x - y$ displacement for sine+Bo field $T = 10k/\sqrt{E}$ (normalized for now) plotted for $\sqrt{E}$ vs. ξ.

transition at $\sqrt{E} = 19.0$ remains plausible in this case also. There is one more drop to normal diffusion after this energy, but it does seem that at this energy the behavior of the profile has changed.

We also can examine the behavior of the EB profile shown in the bottom part of Fig. 3-8. The EB allows to quickly determine the characteristics of the TA MSD ensemble at a given energy, in that we can differentiate between ensembles with small $EB < 1$ (weak ergodicity breaking) or large $EB > 1$ (strong ergodicity breaking) spread like Fig. 3-3 or Fig. 3-4 respectively. Unlike the b profile, the EB fluctuates greatly across the entire energy range. Although the b profile at $\sqrt{E} > 25.0$ flattens out, the EB profile does not. There is a very rough corespondance with high b and strong ergodicity breaking, seen for example at $\sqrt{E} = 9.0$ or 20.0. This is not conclusive however. We would need to explore the effects such as a greater number of particles in the ensemble. Overall, the EB or spread in the TA MSD seems to be influenced by different physics than the b parameter.

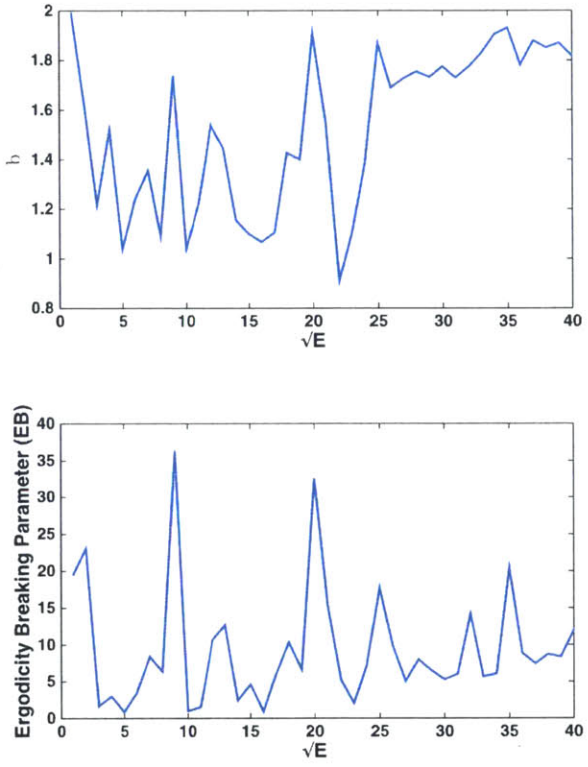

Figure 3-8: The top plot shows the exponent b vs. $\sqrt{E}$, taken in integer steps of $\sqrt{E}$. The second plot shows the ergodicity breaking parameter (EB), a measure of the variance of the ensemble average of individual TA MSD.

Chapter 4

Time Dependent Sine Field

We now explore the effects of time-dependent perturbations superimposed on a background field. As introduced before, charged particles are accelerated in various astrophysical environments. Cosmic rays for example have been observed at very high energies. Previous work on particle energization in three dimensional, time dependent force-free fields has been conducted by [14], using a time varying ABC magnetic field, with $A = B = C = 1$. We not only take different ABC coefficients, but also we use the sine field, which does not contain any integrable regions, and also apply a constant magnetic field.

We add an overall time sinusoidal time dependence to the sine field

$$\mathbf{B} = ((A\sin z)\hat{x} + (B\sin x)\hat{y} + (C\sin y + Bo)\hat{z})\cos(\omega t) = \mathbf{B}_{static}\cos(\omega t) \tag{4.1}$$

The time dependence appears in two of Maxwell's equations, one simply in Faraday's law and the other as the so-called displacement current. We can ignore the displacement current term $\frac{\partial \mathbf{E}}{\partial t}/c^2$ where c is the speed of light, as we will only consider systems changing much slower than the scale set by the speed of light (or in other words, c is effectively infinite).

To find the induced electric field E it is easiest to begin with the time dependent ABC field result and use it to guess a solution to the time dependent sine field.

Following [14] we solve for E_{ABC}, by exploiting the property $\nabla \times B_{ABC} = \lambda B_{ABC}$ and find the result

$$\nabla \times \mathbf{E}_{ABC} = -\frac{\partial\, \mathbf{B}}{\partial t} = -\mathbf{B}\omega \sin(\omega t) = \nabla \times -\frac{\omega}{\lambda}\mathbf{B}_{ABC}\sin(\omega t) \tag{4.2}$$

Now we drop the terms that originated from cosine $\mathbf{B}$ terms (i.e. the spatial sine terms in E_{ABC}) and introduce undetermined multiplicative coefficients for each component,

$$\mathbf{E} = (c_1 \cos(y)\hat{x} + c_2 \cos(z)\hat{(y)} + c_3 \cos(x)\hat{z})\sin(\omega t) \tag{4.3}$$

Now we enforce $\nabla \times \mathbf{E} = -\frac{\partial \mathbf{B}}{\partial t}$ and arrive at the solution

$$\mathbf{E} = \frac{\omega}{\lambda}(C\cos(y)\hat{x} + A\cos(z)\hat{(y)} + B\cos(x)\hat{z})\sin(\omega t) \tag{4.4}$$

Following the previous normalization of the Lorentz equation (Eq. 2.6), in particular $t = \Omega\tau$, we include the electric field term

$$\begin{aligned} \frac{d\mathbf{v}}{d\tau} &= \frac{\lambda}{\Omega}\mathbf{E} + \mathbf{v} \times \mathbf{B} \\ &= \frac{\omega}{\Omega}(C\cos(y)\hat{x} + A\cos(z)\hat{y} + B\cos(x)\hat{z})\sin(\frac{\omega}{\Omega}\tau) + \mathbf{v} \times \mathbf{B} \end{aligned} \tag{4.5}$$

We consider only the case of Alfen waves, where the electric field oscillation frequency ω is much less than the gyrofrequency Ω. Here we take $\frac{\omega}{\Omega} = 0.1$.

As before, we evolve the particles to $300k$ orbits for $\sqrt{E} = 0.01, 0.1, 1.0, \text{and} 10.0$ and calculate the ensemble averaged TA MSD $\langle\overline{\delta^2}\rangle$. Similarly, we also calculate the time averaged 'displacement' in energy $\langle\overline{\delta E^2}\rangle$ in an analogous fashion.

Table 4.1 shows the resulting exponent b for spatial and energy diffusion with the pure sine field and with the constant field added. To first order, we expect there to be little difference in the energy diffusion when the constant field is added because the constant field does not contribute to the induced electric field. We find that the diffusion regime between these two systems has similar characteristics, but are still

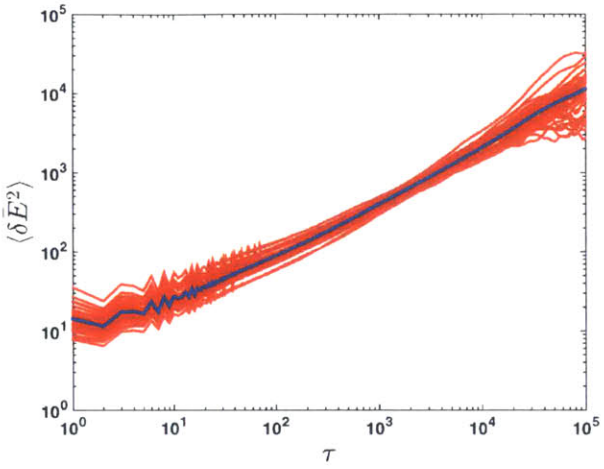

Figure 4-1: Pure sine field: $\langle \overline{\delta E^2} \rangle$ for initial $\sqrt{E} = 0.01$ in blue. The individual $\overline{\delta E^2}$ are in red.

distinctly different.

For the time varying pure sine field, there is a single sub-diffusive energy regime across the order of magnitude initial energies considered, with the exponent b around 0.7. With the background field added, for energies $\sqrt{E} < 10.0$ there is little energy diffusion except at large time scales, as shown in Fig. 4-2. At time scales less than 10^4, there is very little energization. Once it reaches the saturation point, it remains oscillating there for a long time. Overall, as the time scale increases overall the spread in energies decreases, and the average energy slowly increases. There is a large time region that looks like it becomes normal ($b \approx 1.0$), for all the initial energies tested. This regime occurs at time $\tau > 10^4$, so larger time scales are needed to accurately identify the characteristics. For high energies, there is no long time oscillation in the saturation region. The energy TA MSD exhibits a short saturation period at 100 orbits, before entering the diffusive regime.

It is also worth noting that there is a change in the spatial diffusion characteristics for the pure sine field. For the time independent system, there is essentially normal diffusion; however, for the time independent system, there is instead superdiffusion with $b \approx 1.7$.

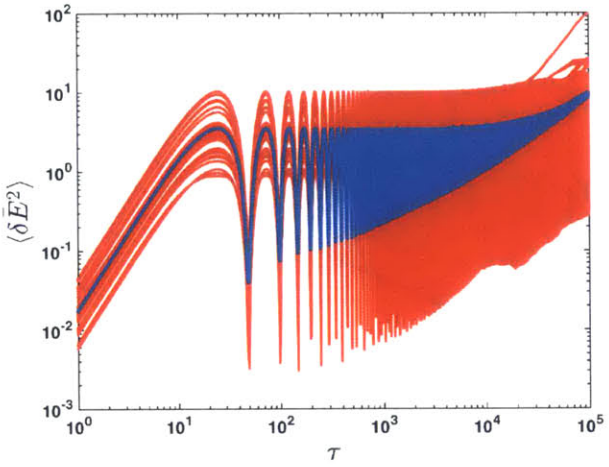

Figure 4-2: Sine + Bo : $\langle \overline{\delta E^2} \rangle$ for initial $\sqrt{E} = 0.01$ in blue. The individual $\overline{\delta E^2}$ are in red.

Table 4.1: Parameters of the form Eq. 2.9 for $\langle \overline{\delta^2} \rangle$ and $\langle \overline{\delta E^2} \rangle$

	Sine XY MSD		Sine + Bo MSD		Sine Energy MSD		Sine + Bo Energy MSD	
$\sqrt{E}$	Onset	b	Onset	b	Onset	b	Onset	b
0.01	10^3	1.71	10^2	1.91	10^2	0.74	5×10^4	0.86
0.1	10^3	1.77	10^2	1.89	10^2	0.76	5×10^4	1.00
1.0	10^3	1.80	10^2	1.89	10^2	0.77	5×10^4	0.92
10.0	10^3	1.81	10^3	1.67	10^1	0.70	10^4	0.96

Chapter 5

Conclusion

We have found the anomalous cross field transport of particles in the sine magnetic field, with and without a constant background field. For the pure sine field, we find evidence of chaotic behavior of the field lines and the particles, as noted by the largest Lyapunov exponent (LE) greater zero. For low energies the LE generally did not depend strongly on the initial conditions of spatial location and velocity orientation, as expected in a chaotic system. However, for $\sqrt{E} = 10.0$ we do find a dependence on the initial conditions.

Furthermore, on diffusive timescales we find that the Larmor radius sets the scale in the sine field system. The low energy particle ensemble, with $R_{max} << 2\pi$, has the time exponent $b \approx 1.0$, which is closer to normal diffusion than in the ABC field. The field lines themselves are slightly superdiffusive. Thus, the particle diffusion and field line diffusion are quite similar in this case. In contrast, the high energy particle ensemble, with $R_{max} > 2\pi$, experiences a near ballistic trajectory.

With the addition of a constant magnetic field, the Larmor radius no longer completely sets the scale of the system. On diffusive scales the constant magnetic field introduces a soft barrier in the TA MSD. When the particles reach the saturation value in the TA MSD, they temporarily saturate, before continuing to diffuse out. The timescale at which the saturation occurs differs according to parameters such as the energy, but the magntiude of the TA MSD at which it saturates does not differ between different parameters. In the final diffusive region, we find the that the

statistics can be dominated by outliers. In Fig. 3-5 for example, most of the particles completely saturate, but a few only temporarily experience saturation, before continuing to follow ballistic motion. In fact, from $\sqrt{E} = 1.0$ to 20.0 there is a large variation in the cross field diffusive properties, jumping between high superdiffusion and normal diffusion. After $\sqrt{E} = 20.0$ there is much more uniformity across the energies, with $b \approx 1.8$. This indicates a clear structure in te parameter space. In Fig. 3-7 we see that the highly variable b region corresponds to regions with uniform particle displacement, and that the uniform b region corresponds to a region of non-uniform particle displacement. In this region of non-uniform displacement there are particles with extremely low displacement and high displacement. These structures are not transient phenomena as they begin early in the particle motion and last into the diffusive regimes.

Furthermore, we find that with a time dependent sine field, there is subdiffusion in energy in the pure sine field, and possible normal diffusion when the constant field is added, indicating that the background field increases energization, even though it does not contribute to the induced electric field. It is necessary to examine larger time scales when the background field is added to more accurately determine what the energy diffusion characteristics of the particles.

Bibliography

[1] V. Archontis. Linear, Non-Linear and Turbulent Dynamos. *Ph.D. Thesis*, January 2000.

[2] V. I. Arnold and B. A. Khesin. Topological Methods in Hydrodynamics. *Annual Review of Fluid Mechanics*, 24(1):145–166, 1992.

[3] Eli Barkai. Anomalous Kinetics Leads to Weak Ergodicity Breaking. In habil Rainer Klages, Gnter Radons, and Igor M. Sokolov, editors, *Anomalous Transport*, pages 213–240. Wiley-VCH Verlag GmbH & Co. KGaA, 2008.

[4] D. P. Bezruchko and D. Smirnov. *Extracting Knowledge From Time Series.* Springer, 2010.

[5] J. Bouchaud. Weak ergodicity breaking and aging in disordered systems. *Journal de Physique I*, 2(9):1705–1713, 1992.

[6] Stas Burov, Jae-Hyung Jeon, Ralf Metzler, and Eli Barkai. Single particle tracking in systems showing anomalous diffusion: the role of weak ergodicity breaking. *Physical Chemistry Chemical Physics*, 13(5):1800, 2011. arXiv: 1009.4846.

[7] Francis F. Chen. *Introduction to Plasma Physics and Controlled Fusion.* Plenum Press, 2 edition, 1983.

[8] T. Dombre, U. Frisch, M. Henon, J. M. Greene, and A. M. Soward. Chaotic streamlines in the ABC flows. *Journal of Fluid Mechanics*, 167:353–391, June 1986.

[9] P. G. Drazin and N. Riley. *The Navier-Stokes Equations: A Classification of Flows and Exact Solutions.* Cambridge, New York, 2006.

[10] J. P. Eckmann and D. Ruelle. Ergodic theory of chaos and strange attractors. *Reviews of Modern Physics*, 57(3):617–656, July 1985.

[11] D. J. Galloway and M. R. E. Proctor. Numerical calculations of fast dynamos in smooth velocity fields with realistic diffusion. *Nature*, 356:691–693, April 1992.

[12] Y. He, S. Burov, R. Metzler, and E. Barkai. Random Time-Scale Invariant Diffusion and Transport Coefficients. *Physics*, 101, July 2008.

[13] E. N. Lorenz. *Turbulence and Predictability in Geophysical Fluid Dynamics and Climate Dynamics.* Academic Press, New York, 1985. pp. 243-265.

[14] Dhrubaditya Mitra, Axel Brandenburg, Brahmananda Dasgupta, Eyvind Niklasson, and Abhay Ram. Particle energization through time-periodic helical magnetic fields. *Physical Review E*, 89(4), April 2014. arXiv: 1306.0151.

[15] Radu Balescu. Strange Diffusion. *Condens. Matter Phys*, 1(4):815–833, 1998.

[16] Abhay K. Ram, Brahmananda Dasgupta, V. Krishnamurthy, and Dhrubaditya Mitra. Anomalous diffusion of field lines and charged particles in Arnold-Beltrami-Childress force-free magnetic fields. *Physics of Plasmas (1994-present)*, 21(7):072309, July 2014.

[17] S.M. Rytov, Yu A. Kravtsov, and V. I. Tatarskii. *Principles of Statistical Radiophysics 1: Elements of Random Process Theory.* Springer-Verlag, 2 edition, July 1987.

[18] Loukas Vlahos, Heinz Isliker, Yannis Kominis, and Kyriakos Hizanidis. Normal and Anomalous Diffusion: A Tutorial. *arXiv:0805.0419 [nlin]*, May 2008. arXiv: 0805.0419.

[19] Thomas Wiegelmann and Takashi Sakurai. Solar Force-free Magnetic Fields. *Living Reviews in Solar Physics*, 9, 2012.